Title

Approximate solution for seismic earth pressures on rigid walls retaining inhomogeneous elastic soil

Authors

Brandenberg, Scott J
Mylonakis, George
Stewart, Jonathan P

Publication Date

2017-06-01

DOI

10.1016/j.soildyn.2017.03.028

Peer reviewed

Approximate Solution for Seismic Earth Pressures on Rigid Walls Retaining Inhomogeneous Elastic Soil

Scott J. Brandenberg[1], George Mylonakis[2], and Jonathan P. Stewart[3]

Abstract: An approximate elasto-dynamic solution is developed for computing seismic earth pressures acting on rigid walls retaining continuously inhomogeneous elastic material and excited by vertically propagating shear waves. The shear modulus of the soil is represented as a nonlinear function of depth, in a manner that is consistent with established analytical and empirical relationships, while mass density and Poisson's ratio are assumed constant. Solutions are presented for a single wall and for a pair of walls spaced at a finite distance. A shape function characterizing the vertical variation of horizontal displacement of the soil column in the free-field is assigned, and simplifying assumptions regarding the dynamic vertical stresses and the vertical-to-horizontal displacement gradient are made to facilitate closed-form expressions for horizontal displacement and stress fields. These solutions are used to compute the distribution of dynamic horizontal earth pressure acting on the wall. A Winkler stiffness intensity relationship is then derived such that the proposed method can be extended beyond the boundary conditions considered herein. These solutions agree well with exact analytical elasto-dynamic solutions for inhomogeneous soil that are considerably more complicated to implement. Causes of differences between the solutions are discussed.

Keywords: seismic earth pressure; retaining structure; inhomogeneous soil; dynamic analysis.

[1] Associate Professor, Department of Civil and Environmental Engineering, 5731 Boelter Hall, Univ. of California, Los Angeles, CA 90095-1593 (corresponding author). E-mail address: sjbrandenberg@ucla.edu
[2] Professor and Chair in Geotechnics and Soil-Structure Interaction, Dept. of Civil Engineering, Clifton BS8, Bristol, U.K.; Professor, Univ. of Patras, Greece; Adjunct Professor, Dept. of Civil and Environmental Engineering, 5731 Boelter Hall, Univ. of California, Los Angeles, CA 90095-1593. Email: g.mylonakis@bristol.ac.uk
[3] Professor and Chair, Dept. of Civil and Environmental Engineering, 5731 Boelter Hall, Univ. of California, Los Angeles, CA 90095-1593. E-mail: jstewart@seas.ucla.edu

1. Introduction

Seismic earth pressures acting on embedded walls are most commonly analyzed using a limit equilibrium concept originally developed by Okabe [1] and Mononobe and Matsuo [2], commonly known as the Mononobe-Okabe (M-O) method. The M-O method was subsequently modified in various manners (e.g., [3], [4], [5], [6]). This family of methods (referred to as limit state methods) assumes that an inertia force acts on an active wedge to produce a dynamic increment of earth pressure.

Limit state methods overlook several important aspects of the problem, such as wave propagation, poroelasticity of saturated soils (e.g., [7], [8], [9]), and soil-structure interaction that produces mismatches between wall and free-field soil displacements. Inertial forces in the backfill do not load the wall directly, as assumed in limit state methods. To illustrate this point, consider an embedded wall with the same mass and stiffness as the soil. Vertically propagating shear waves will induce no increment of lateral seismic earth pressure because inertia forces are transmitted entirely by shear, in accordance with the solution for one-dimensional shear wave propagation. Hence, there is no fundamental association between backfill inertia and seismic wall pressures.

In a realistic wall-soil system (with wall elements stiffer than those for soil), dynamic body forces in the backfill induce dynamic deformations, which are incompatible with wall kinematics, causing interaction stresses to develop between the wall and soil. Furthermore, inertial loads arising from differences in mass between the wall structure and soil, or from the dynamic response of an above-ground structure attached to the wall, will produce force and overturning demands on the wall that in turn induce relative deformations and seismic earth pressures at wall-soil interfaces. As these phenomena are overlooked in limit analysis, M-O type methods fail to properly capture the fundamental physics of soil-wall interaction.

It is therefore not surprising that the literature is mixed on the accuracy of the M-O method and its variants. Recent experimental studies have challenged the M-O method as being overly conservative for cantilever U-shaped walls [10] and free-standing retaining walls [11], and as providing a reasonable upper-bound for braced walls [12]. By contrast, analytical elasto-dynamic solutions [13], [14] and numerical modeling studies [15] have challenged M-O as being unconservative. This has led to confusion among practicing engineers and researchers regarding appropriate methods of analysis.

Brandenberg et al. [16] developed an elasto-dynamic Winkler-based framework for the kinematic wall-soil interaction problem that explains both the lower-than-M-O experimental observations and the higher-than-M-O analytical and numerical simulations. The key parameter controlling relative wall-soil displacements, and hence mobilized earth pressures, is the ratio of wavelength, λ, of the vertically propagating shear wave, to wall height, H, which can be interpreted as a dimensionless frequency. Walls founded on thick soil deposits (like the experimental studies and most retaining structures) tend to have high λ/H ratios, which are associated with modest depth-dependent free-field displacements that are largely followed by wall-foundation systems. Under such conditions, earth pressures are low for a given surface motion amplitude. In contrast, the response of a uniform soil deposit resting on a rigid base is often dominated by the first mode of horizontal vibration, which corresponds to $\lambda/H = 4$ for retained soil deposits that are long relative to their thickness. Rigid walls resting on a rigid base (as often assumed in elasto-dynamic solutions) can therefore mobilize significant kinematic interaction and high earth pressures.

Although the Brandenberg et al. [16] solutions explain several key features of behavior, assumptions that limit their applicability include (1) uniform shear modulus with depth, (2) rigid walls, (3) a lack of gapping at the soil-wall interface, and (4) elastic soil behavior. The purpose of this paper is to address the assumption of uniform shear modulus with depth. To this end, an approximate elasto-dynamic

solution is developed for continuously inhomogeneous soil, defined as a soil layer with a smooth variation of shear modulus with depth (as opposed to layers with abrupt transitions in shear modulus), using simplifications similar to those employed by Kloukinas et al. [17]. An expression for equivalent Winkler stiffness intensity is developed, and the solutions are compared with more rigorous numerical formulations from the literature.

2. Vertical variation of soil shear modulus

A number of empirical and theoretical equations have been suggested to capture the dependence of soil shear modulus on mean effective stress. Hertz [18], in his landmark 1882 paper, derived an expression in which the shear modulus of a particulate medium composed of elastic spheres is proportional to the mean effective stress raised to a power, n, which he found equal to 1/3. The same result was later obtained by more elaborate, yet still idealized particle contact models. Hardin and Richart [19] suggest a form in which the shear modulus is also a function of void ratio. Building upon the earlier work by Mindlin et al. [20], Hardin and Drnevich [21] found experimentally that $n = 0.5$ and also introduced an overconsolidation ratio term for plastic soils. Yamada et al. [22] also recommend $n = 0.5$ for granular soils and suggested that $n = 1$ for plastic clay-sand mixtures (they did not include a void ratio term in their formulation, which may explain why n is higher). All of these forms result in zero shear modulus when the effective stress is zero, which is unrealistic as it does not account for cementation, cohesion, capillary effects, and can be numerically problematic near the surface.

Although shear modulus fundamentally depends on effective stress, it has also conveniently been formulated as a function of depth to facilitate analytical solutions. For example, Wood [13] and Veletsos and Younan [23] formulated solutions for the seismic increment of lateral earth pressure exerted by a soil deposit with a parabolic variation of shear modulus with depth, $G(z)$. Rovithis et al. [24] suggest a form for shear wave velocity as a function of depth, $V_s(z)$, that is equivalent to the equation for $G(z)$ in

Eq. 1 for mass density, ρ = const., where z is depth, z_r is a reference depth, G_r is the shear modulus at z = z_r, and b is a constant that influences the depth gradient and the value of $G_0 = G(0)$ (note that $G_0 = G_r b^{2n}$). Rovithis et al. [24] utilize n for the depth-variation of V_s rather than for G, and it is therefore multiplied by 2 here to represent G. Their application was vertical wave propagation through a vertically inhomogeneous layer resting on a rigid base.

$$G(z) = G_r \left[b + (1-b)\frac{z}{z_r} \right]^{2n} = G_r f(z) \tag{1}$$

Vrettos et al. [25] utilized the form provided in Eq. 2, where G_∞ is the modulus at an infinite depth (approached asymptotically as $z \longrightarrow \infty$), and η is a constant that controls the rate of change of G with depth. Using this form, Vrettos et al. [25] developed exact analytical solutions for the response of a continuously inhomogeneous soil layer on a rigid base restrained between two rigid walls subjected to horizontal base shaking (illustrated in Fig 1b).

$$G(z) = G_0 + (G_\infty - G_0)\left(1 - e^{-\eta z/H}\right) \tag{2}$$

In this paper, we formulate an approximate analytical solution for seismic earth pressure following the approach developed by Kloukinas et al. [17], but for soil with vertically inhomogeneous shear modulus resting on a rigid base (Fig. 1). The functional form for vertical inhomogeneity of shear modulus follows Rovithis et al. [24]. Solutions are developed for a single rigid wall retaining an infinitely long soil deposit (Fig. 1a) and for two rigid walls retaining a finite length deposit (Fig. 1b) (the common case of basement

walls, with soil pressures on the outside, would be analyzed using the geometry in Fig 1a). The resulting earth pressures are compared with the exact analytical solutions formulated by Vrettos et al. [25]. The rigid wall and rigid base boundary conditions facilitate development of an analytical solution, but do not correspond well to most practical problems (the rigid base being a particularly strong limitation, although one that is very common in analytical and numerical solutions for retaining wall response). With an eye towards applications in which these limitations are relaxed, we also develop Winkler stiffness parameters suitable to solutions for flexible walls retaining vertically inhomogeneous soil and resting on a compliant base (a condition for which continuum analytical solutions are exceptionally difficult). We recognize that Winkler solutions for flexible walls and/or flexible base conditions are of the greatest practical use; such solutions are under development and are not presented here. This paper presents the admittedly intermediate, though essential, development of the elasto-dynamic solution and formulation of Winkler stiffness intensity for the case of inhomogeneous soil.

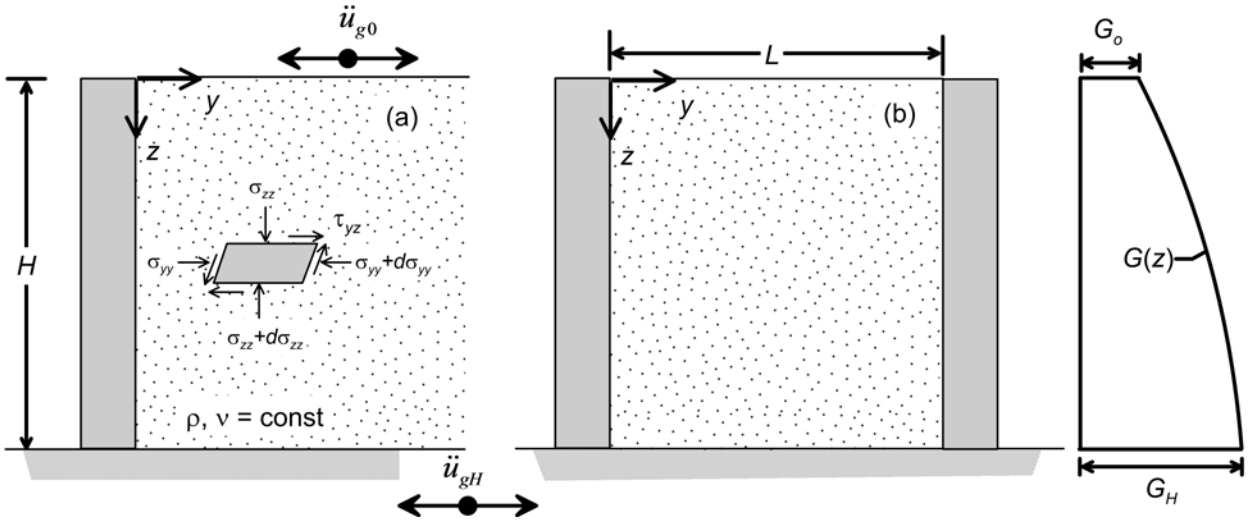

Figure 1. Vertically heterogeneous soil retained (a) by a single rigid wall, and (b) between a pair of rigid walls.

3. Equation of motion

The equation of motion derived from horizontal equilibrium of the element in Fig. 1 is provided in Eq. 3, where stress components correspond to the changes induced by the imposed ground motion and do not include initial static stresses.

$$\frac{\partial \sigma_{yy}}{\partial y} + \frac{\partial \tau_{yz}}{\partial z} + \rho \frac{\partial^2 u_y}{\partial t^2} = \rho \ddot{u}_{gH} \tag{3}$$

Stresses σ_{yy} and τ_{yz} are defined in Fig. 1, variable u_y indicates horizontal displacement in the y direction relative to the base, and $\ddot{u}_{gH}$ is horizontal acceleration at the base of the deposit.

Isotropic elasticity theory for plane strain conditions provides equations for the applicable stress components given by Eq. 4, where *f* is the function of depth from Eq. 1.

$$\sigma_{yy} = \frac{2G_H f}{1-2\nu}\left[(1-\nu)\frac{\partial u_y}{\partial y} + \nu \frac{\partial u_z}{\partial z}\right] \tag{4a}$$

$$\sigma_{zz} = \frac{2G_H f}{1-2\nu}\left[(1-\nu)\frac{\partial u_z}{\partial z} + \nu \frac{\partial u_y}{\partial y}\right] \tag{4b}$$

$$\tau_{yz} = G_H f\left(\frac{\partial u_y}{\partial z} + \frac{\partial u_z}{\partial y}\right) \tag{4c}$$

Following Veletsos and Younan [14] and Kloukinas et al. [17], we assume that the increment in vertical normal stress due to horizontal shaking is zero ($\sigma_{zz} = 0$) and that the derivative of vertical soil displacements with horizontal distance from the wall is also zero $\left(\frac{\partial u_z}{\partial y} = 0\right)$ everywhere in the soil

domain. The validity of these approximations is discussed in the aforementioned publications. Also, setting $z_r = H$ (and hence $G_r = G_H$), and making appropriate algebraic substitutions into Eq. 3, the equation of motion may be represented by Eq. 5, where $\Psi_e^2 = (2\text{-}\nu)/(1\text{-}\nu)$ and ω is angular frequency. Note that the complex shear wave velocity at the base of the deposit $V_H^* = V_H\sqrt{1+2iD}$ may be utilized in Eq. 5 to account for linear hysteretic material damping ratio, D.

$$\psi_e^2 f \frac{\partial^2 u_y}{\partial y^2} + \frac{\partial f}{\partial z}\frac{\partial u_y}{\partial z} + f \frac{\partial^2 u_y}{\partial z^2} + \frac{\omega^2}{V_H^2} u_y = \frac{\ddot{u}_{gH}}{V_H^2} \tag{5}$$

Note that due to the approximate nature of the analysis involved, equilibrium in the vertical direction is not satisfied in this approach, nor is the soil surface completely free of shear tractions. In the same vein, the wall is neither perfectly rough nor perfectly smooth [14]. However, as shown in the aforementioned publications and in results presented below, these approximations typically have a minor influence on the resulting solution.

4. Proposed solution

Our approach to the solution of vertical distribution of stress on the walls is to first determine the applicable ground displacements by solving the equation of motion (Eq. 5). Those displacements are then used in Eq. 4 to compute stresses. Following the principal of virtual work, the variational form of Eq. 5 is represented by Eq. 6, where the $\Phi(z)$ is a predefined dimensionless weight function that must satisfy the essential boundary condition $\Phi(H) = 0$.

$$\psi_e^2 \int_0^H f \frac{\partial^2 u_y}{\partial y^2}\Phi dz + \int_0^H \frac{\partial f}{\partial z}\frac{\partial u_y}{\partial z}\Phi dz + \int_0^H f \frac{\partial^2 u_y}{\partial z^2}\Phi dz + \int_0^H \frac{\omega^2}{V_H^2} u_y \Phi dz = \frac{\ddot{u}_{gH}}{V_H^2}\int_0^H \Phi dz \tag{6}$$

The third term on the left-hand side is integrated by parts as in Eq. 7.

$$\int_0^H f\,\frac{\partial^2 u_y}{\partial z}\Phi dz = f\,\frac{\partial u_y}{\partial z}\Phi\Big|_0^H - \int_0^H \frac{\partial u_y}{\partial z}\left(\frac{\partial f}{\partial z}\Phi + f\,\frac{\partial \Phi}{\partial z}\right)dz \tag{7}$$

In light of the essential boundary condition $\Phi(H) = 0$, and the natural boundary condition $du_y/dz = 0$ at z = 0 due to the absence of shear tractions at the surface, the first term on the right hand side of Eq. 7 must be zero.

Following [17], we represent the horizontal displacement in a separable form using Eq. 8, where $Y(y)$ is an unknown function of horizontal distance from the wall, having dimensions of length, and $\Phi(z)$ is a trial function [referred to subsequently as a "shape function" following finite element convention (e.g.,[26]), taken here as having the same form as the weight function.

$$u_y(y,z) = Y(y)\Phi(z) \tag{8}$$

Substituting Eqs. 7 and 8 into Eq. 6 results in Eq. 9, which is the so-called weak form of the governing differential equation.

$$\left(H\psi_e\right)^2 \frac{\partial^2 Y}{\partial y^2} - b_{oc}^2\left(a_{oc}^2 - a_o^2\right)Y = \frac{H^2\mathcal{L}}{V_H^{\,2}}\ddot{u}_{gH} \tag{9}$$

where

$$a_o = \frac{\omega H}{V_H} \tag{10a}$$

$$a_{oc}^2 = H^2 \int_0^H f \left(\frac{d\Phi}{dz} \right)^2 dz \Big/ \int_0^H \Phi^2 dz \tag{10b}$$

$$b_{oc}^2 = \int_0^H \Phi^2 dz \Big/ \int_0^H f \Phi^2 dz \tag{10c}$$

$$\mathcal{L} = \int_0^H \Phi dz \Big/ \int_0^H f \Phi^2 dz \tag{10d}$$

The parameter a_o is a dimensionless frequency, and a_{oc} is an approximation of the fundamental dimensionless frequency of the soil deposit which can be interpreted as a "cutoff" frequency beyond which horizontally propagating stress waves emerge in the retained soil. The value of a_{oc} is exact if Φ is selected to match the displacement profile corresponding to the fundamental mode. Parameter $\mathcal{L}$ on the right-hand side is a modal participation coefficient. Finally, b_{oc} is a stiffness multiplier resulting from the inhomogeneity of the medium. Note that $f = 1$ (and therefore $b_{oc} = 1$) for homogeneous soil, in which case the above parameters reduce to those in the Kloukinas et al. [17] solution. The presence of parameter b_{oc} and function f in Eqs. 9 and 10 distinguishes the proposed solution from the earlier one by Kloukinas et al. [17].

The shape function must satisfy the essential boundary condition $\Phi(H) = 0$, and it must be at least once differentiable with respect to z. However, it need not satisfy the natural boundary condition $\Phi'(0) = 0$ because this was directly imposed in deriving the weak form. In this light, the strong and weak forms on the two sides of Eq. 7 could be unequal, with the weak form on the right side being preferred. This is an important element of the analysis, since the error introduced in the solution by the approximate shape

function greatly reduces as the order of differentiation decreases. This allows the use of "imperfect" shape functions that don't satisfy the higher-order derivatives at the boundaries, such as the linear shape function employed by Kloukinas et al. [17]. Furthermore, the gradient $d\Phi/dz$ is not meaningful when evaluated at isolated points, but only in an integral sense (note that gradients of Φ appear only inside integrals in Eqs. 10b, 10c, and 10d). Scott [27] discusses related techniques, as applied to classical foundation engineering problems. Applications to foundation dynamics have been presented by Mylonakis [28] and Anoyatis and Lemnitzer [29].

4.1 Solution for single wall

For a single wall retaining a deposit of soil that extends infinitely in the positive y-direction, the boundary conditions for Eq. 9 are $Y(0) = 0$, and $Y(\infty)$ = finite. The elementary solution is given by Eq. 11. The total solution for soil displacement relative to the base is obtained by multiplying Eq. 11 by $\Phi(z)$.

$$\mathrm{Y(y)} = -\frac{\boldsymbol{\mathcal{L}}}{b_{oc}^2\left(a_{oc}^2 - a_o^2\right)}\frac{\rho H^2 \ddot{u}_{gH}}{G_H}\left[1 - \exp\left(-\frac{1}{\psi_e} b_{oc}\sqrt{a_{oc}^2 - a_o^2}\,\frac{y}{H}\right)\right] \tag{11}$$

The horizontal pressure acting on the rigid wall is obtained at $y = 0$, by making appropriate substitutions into Eq. 4a, and is given by Eq. 12, where $\psi_\sigma = 2\Big/\sqrt{(2-\nu)(1-\nu)}$.

$$\sigma_{yy}(0,\mathrm{z}) = -\frac{\psi_\sigma \boldsymbol{\mathcal{L}} \rho H \ddot{u}_{gH}}{b_{oc}\sqrt{a_{oc}^2 - a_o^2}}\, f\Phi \tag{12}$$

The pressure resultant, P_E, is obtained by integrating the horizontal pressure over the wall height, as indicated in Eq. 13.

$$P_E = -\frac{\psi_\sigma \, \mathcal{L} \rho H \, \ddot{u}_{gH}}{b_{oc}\sqrt{a_{oc}^2 - a_o^2}} \int_0^H f\,\Phi dz \tag{13}$$

Finally, the height of the resultant above the base of the wall, *h*, is computed using Eq. 14.

$$\frac{h}{H} = 1 - \frac{\int_0^H f\,\Phi z dz}{H\int_0^H f\,\Phi dz} \tag{14}$$

Different shape functions produce different solutions because $\mathcal{L}$, a_{oc}, and b_{oc} depend on $\Phi(z)$. The shape function adopted here (Eq. 15) is the exact fundamental mode shape corresponding to the solution by Rovithis et al. [24]. Note that $Z = z/H$, and $J_\alpha()$ and $N_\alpha()$ denote Bessel functions of the first and second kind of order α, respectively, where $\alpha = (2n\text{-}1)/2(1\text{-}n)$. Solutions for various alternative shape functions are presented in the appendix.

$$\Phi(Z) = \frac{\pi\lambda_0\left[b+(1-b)Z\right]^{(1-2n)/2}}{2b^{-1/2}}\left\{J_{\alpha+1}\left(\lambda_0 b^{1-n}\right)N_\alpha\left[\lambda_0\left(b+(1-b)Z\right)^{1-n}\right] - N_{\alpha+1}\left(\lambda_0 b^{1-n}\right)J_\alpha\left[\lambda_0\left(b+(1-b)Z\right)^{1-n}\right]\right\} \tag{15}$$

In Eq. 15, λ_0 corresponds to the first mode eigenvalue, and is computed by solving the lowest value of λ_0 that satisfies the characteristic equation (Rovithis et al. [24]):

$$J_{\alpha+1}\left(\lambda_0 b^{1-n}\right)N_\alpha\left(\lambda_0\right) - J_\alpha\left(\lambda_0\right)N_{\alpha+1}\left[\lambda_0 b^{1-n}\right] \tag{16}$$

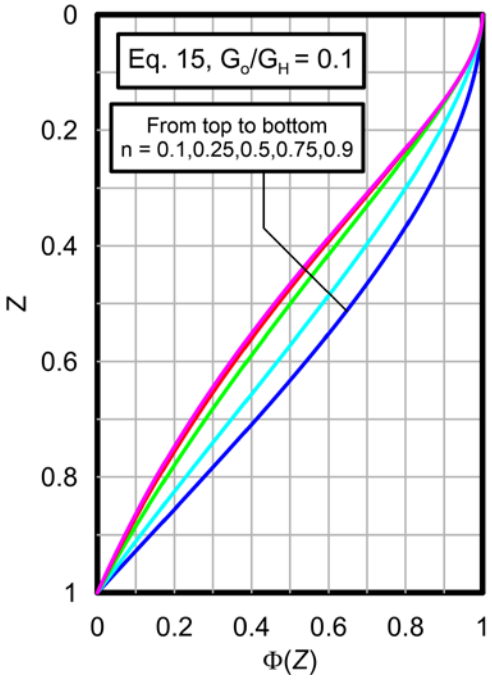

Figure 2. Shape functions corresponding to the exact eigenvectors for one-dimensional wave propagation.

Substituting Eq. 15 into Eqs. 10b and 10c results in long non-integrable expressions. Therefore, the expressions have been integrated numerically, and the results for $\mathcal{L}$, a_{oc}, and b_{oc} are provided in Fig. 3 as functions of n and b. When either $n = 0$ or $b = 1$ (i.e., a uniform profile), $\mathcal{L}$, a_{oc}, are constant and b_{oc} is unity, resulting in a solution equivalent to the expressions for a uniform profile derived by Kloukinas et al. [17]. Differences among the solutions for the various shape functions increase as the degree of inhomogeneity increases (i.e., as n increases or b decreases).

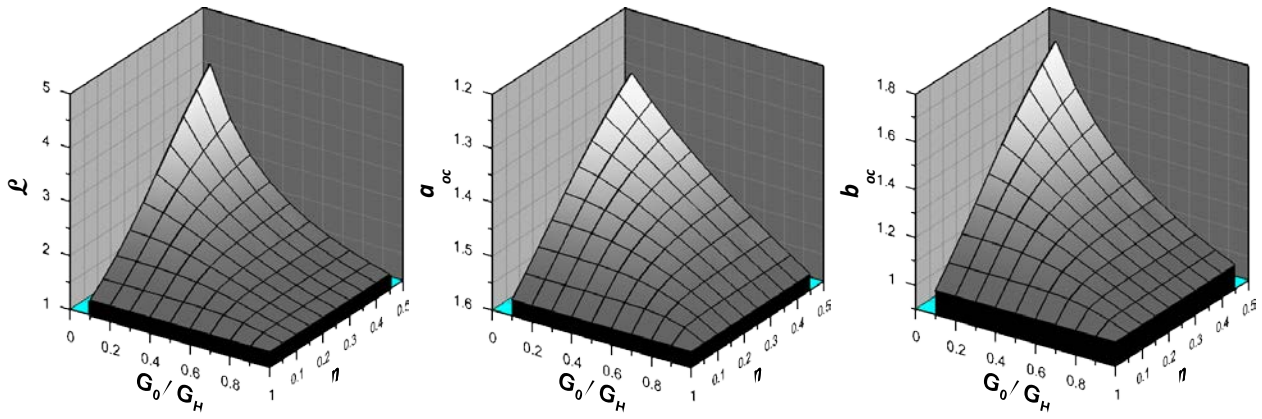

Figure 3. Solutions for $\mathcal{L}$, a_{oc}, and b_{oc} as function of n and G_0/G_H.

For ease of application, we present in Eq. 17 approximate relations for the model parameters developed through least squares regression of the results from Figure 3. These equations provides errors with mean of 0 and standard deviations of 4%, 1%, and 2% for $\mathcal{L}$, a_{oc}, and b_{oc}, respectively, in the range G_0 / G_H = 0.1 to 0.9 and n = 0.05 to 0.45. Note that n = 0.5 corresponds to a parabolic variation of shear wave velocity and linear variation of shear modulus with depth.

$$\mathcal{L} = 6.382 \cdot e^{-2.975\cdot(1-2n)-3.581\cdot b} + 4/\pi \quad (17a)$$

$$a_{oc} = -0.538 \cdot e^{-2.400\cdot(1-2n)-2.348\cdot b} + \pi/2 \quad (17b)$$

$$b_{oc} = 1.492 \cdot e^{-2.603\cdot(1-2n)-3.054\cdot b} + 1 \quad (17c)$$

4.3 Solution for pair of walls

For a soil layer of finite length, *L*, retained between two rigid walls (Fig 1b), the boundary conditions required to solve Eq. 9 are *Y*() = 0, and *Y*(*L*) = 0. (By symmetry, it also holds that $\sigma_{yy}(L/2,z) = 0$, which can be used as an alternative boundary condition.) The elementary solution is given by Eq. 18.

$$\mathrm{Y(y)} = -\frac{\mathcal{L}}{b_{oc}^2\left(a_{oc}^2 - a_o^2\right)}\frac{\rho H^2 \ddot{u}_{gH}}{G_H}\frac{\left[1-\exp\left(-\frac{1}{\psi_e}b_{oc}\sqrt{a_{oc}^2-a_o^2}\,\frac{y}{H}\right)+\exp\left(-\frac{1}{\psi_e}b_{oc}\sqrt{a_{oc}^2-a_o^2}\,\frac{L}{H}\right)-\exp\left(-\frac{1}{\psi_e}b_{oc}\sqrt{a_{oc}^2-a_o^2}\,\frac{L-y}{H}\right)\right]}{1+\exp\left(-\frac{1}{\psi_e}b_{oc}\sqrt{a_{oc}^2-a_o^2}\,\frac{L}{H}\right)} \tag{18}$$

The horizontal pressure acting on the rigid wall is obtained at *y* = 0 by making appropriate substitutions into Eq. 4a, and is given by Eq. 19.

$$\sigma_{yy}(0,\mathrm{z}) = -\frac{\psi_\sigma\,\mathcal{L}\rho H\,\ddot{u}_{gH}}{b_{oc}\sqrt{a_{oc}^2-a_o^2}}\frac{1-\exp\left(-\frac{1}{\psi_e}b_{oc}\sqrt{a_{oc}^2-a_o^2}\,\frac{L}{H}\right)}{1+\exp\left(-\frac{1}{\psi_e}b_{oc}\sqrt{a_{oc}^2-a_o^2}\,\frac{L}{H}\right)}\,f\,\Phi \tag{19}$$

The value of a_{oc} in Eq. 10b was derived for a one-dimensional wave propagation solution, and is consistent with the Rayleigh approach for approximating the natural frequency of the free-field soil deposit [30]. However, this value of a_{oc} may under-estimate the first mode natural frequency for a finite-length deposit because the constraints provided by the rigid walls stiffen the system. A two-dimensional Rayleigh solution may be utilized to provide a more accurate estimate of the dimensionless natural frequency, $\hat{a}_{oc}$, of a finite-length deposit. The two-dimensional Rayleigh solution is provided by Eq. 20. This equation was derived following procedures outlined by Paolucci (1999) [30], and the derivation is omitted for brevity.

$$\hat{a}_{oc}^2 = \frac{2}{1-\nu}\frac{H^2}{b_{oc}^2}\frac{\int_0^L \left(\frac{dY}{dy}\right)^2 dy}{\int_0^L Y^2 dy} + a_{oc}^2 \qquad (20)$$

which is higher than a_{oc}, due the restraining action of the walls at the two ends of the domain.

We present in Figure 4 the ratio $\hat{a}_{oc}/a_{oc}$ plotted versus *L*/*H* for a condition wherein *n* = 0.25, G_0/G_H = 0.5, and ν = 0.3, as well as for an essentially uniform profile (*n* = 0.01, G_0/G_H = 0.99) and an essentially linear profile of shear modulus (*n* = 0.5, G_0/G_H = 0.01). The results in Fig 4 are similar for these different inhomogeneous soil profiles. Furthermore, the solution is nearly insensitive to Φ(z), as the plots for all four shape functions plot essentially on top of each other. The frequency ratio increases sharply as *L*/*H* becomes smaller than about 4, and is nearly equal to unity for *L*/*H* larger than 10 (hence the validity of the one dimensional Rayleigh solution for a single wall).

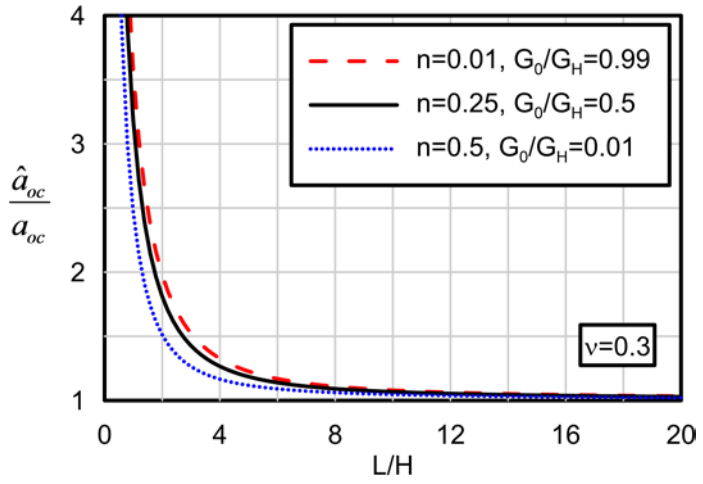

Figure 4. Solution for $\hat{a}_{oc}/a_{oc}$ versus L/H for various combinations of b and n; ν=0.3.

5. Comparison of proposed solution with exact solution

The solutions formulated by Vrettos et al. [25] provide a benchmark to which our simpler approximate analytical solution may be compared. The Vrettos et al. solution is for the two-wall problem in Fig. 1b (no comparable single-wall solution is presented). To facilitate this comparison, the profile of shear modulus given by Eq. 1 must be matched to the profiles of shear modulus utilized by Vrettos et al. [25] given by Eq. 2. We do this by setting the shear modulus at the top and bottom of the profiles to be the same (and thereby solving for *b*), and subsequently computing *n* to achieve the same average shear modulus over the layer thickness. Examples of the matched profiles are shown in Fig. 5.

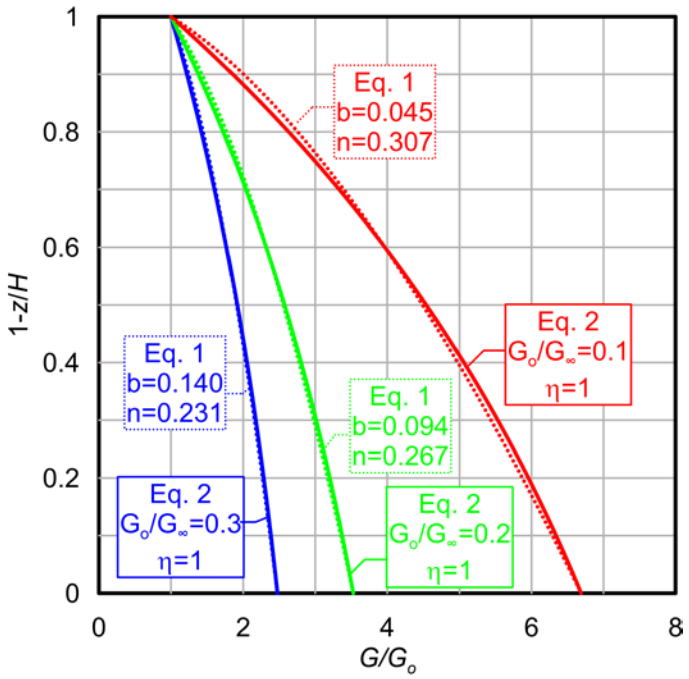

Figure 5. Matched Profiles of normalized shear modulus using Eq. 1 by Rovithis et al. [24] (dotted lines) and Eq. 2 by Vrettos et al. [25] (solid lines).

Earth pressure distributions reported by Vrettos et al. [25] are compared with the proposed solution in Fig. 6 for G_0/G_∞ = 0.1, 0.2, and 0.3 for a range of frequencies and for L/H = 10. Vrettos et al. reported results for selected values of dimensionless frequency $\beta_0 = (\omega H/V_o)^2$; reported solutions are for β_0 = 2.36,

and 5.76 for all three G_0/G_∞ ratios, and also for β_0 = 9 and 12 for G_0/G_∞ = 0.1. The proposed solutions agree reasonably well with the exact solutions, particularly at shallow depths. The proposed solution predicts zero seismic earth pressure at the base of the wall, whereas the exact solution predicts non-zero seismic earth pressure at that depth. The cause of this discrepancy lies in the use of shape function $\Phi(z)$, which is zero at the bottom of the layer, thus rendering as zero the contact stresses at the base of the wall. This can also be viewed as the outcome of a Winkler type solution, given the zero relative displacement between wall and soil at the base of the layer.

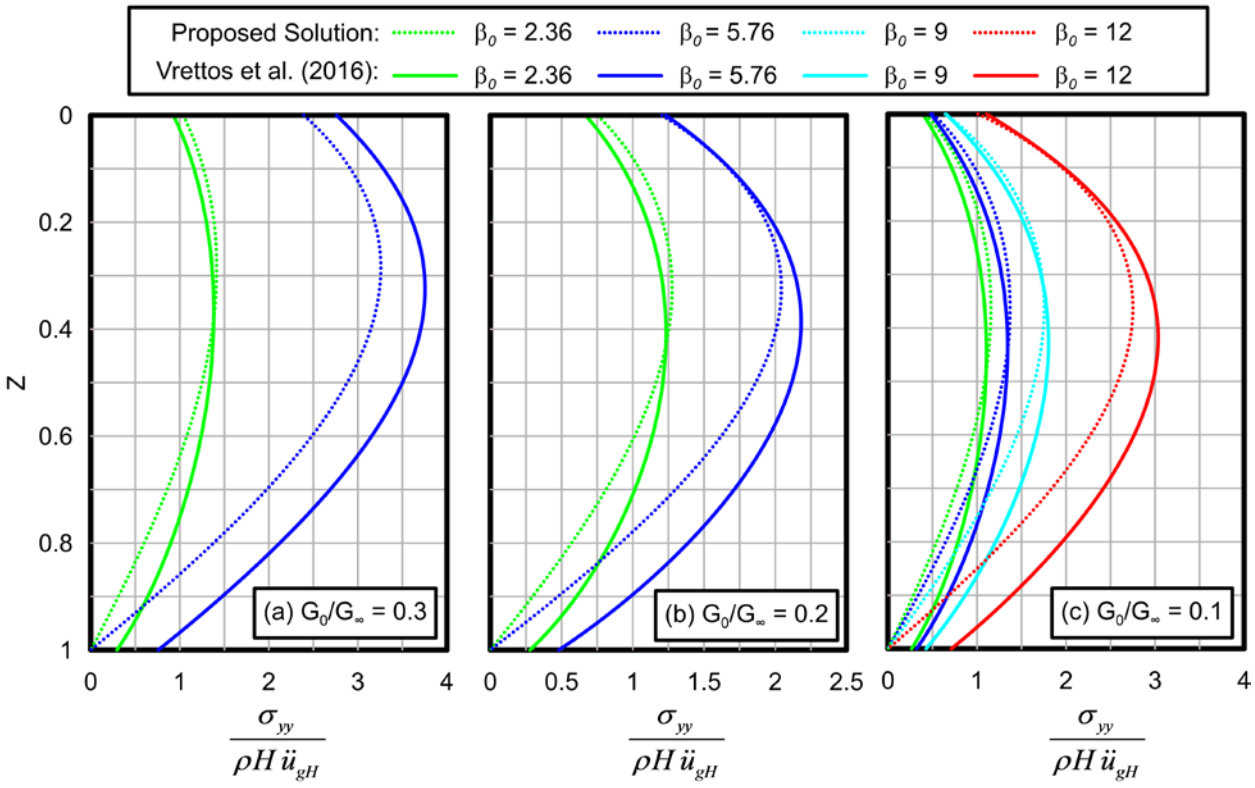

Figure 6. Profiles of normalized earth pressure $\frac{\sigma_{yy}}{\rho H\, \ddot{u}_{gH}}$ for various values of G_0/G_∞ at various dimensionless frequencies. Note that $\beta_0 = (\omega H/V_0)^2$, ν = 0.3, and L/H = 10.

Using the shape function given by Eq. 15d, the normalized seismic thrust versus normalized frequency relationships are presented in Fig. 7 for profiles with G_0/G_∞ = 0.1, 0.2, and 0.3, and for various L/H ratios. These solutions are plotted only up to $a_o/\hat{a}_{oc} = 1$ because the use of first-mode shape functions for Φ renders the solutions inappropriate at frequencies higher than first-mode resonance. The proposed solution tends to under-estimate the Vrettos et al. [21] solution, particularly near resonance (i.e., values of $a_o/\hat{a}_{oc}$ near unity) and lower values of L/H. The under-prediction for low values of L/H may be related to additional modes of vibration in the exact solution that are not being captured by the proposed solution.

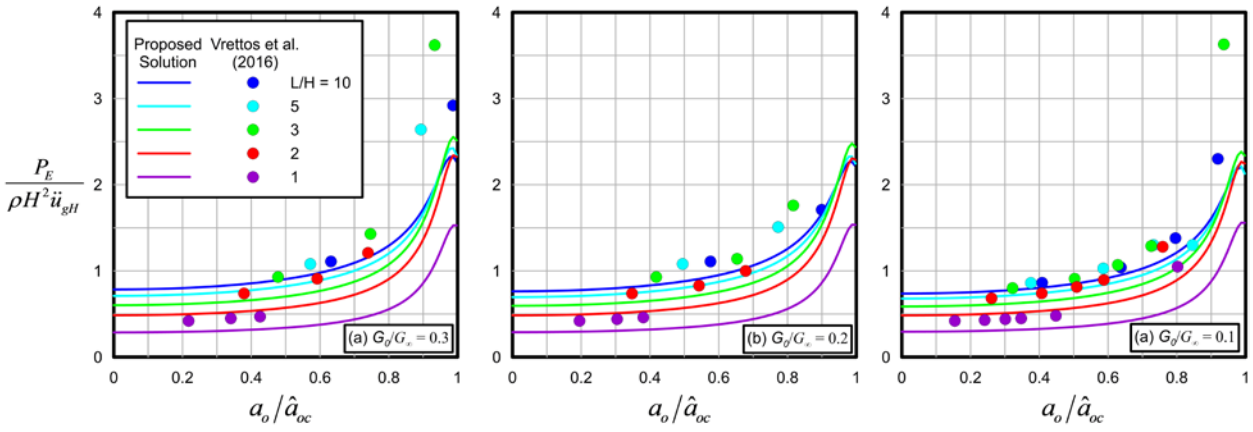

Figure 7. Dimensionless resultant force $\frac{P_E}{\rho H^2 \ddot{u}_{gH}}$ versus dimensionless frequency for proposed solution compared with discrete points tabulated by Vrettos et al. [25] (D = 0.05, ν = 0.3).

6. Winkler stiffness

The pressure mobilized against the wall is assumed to be a function of the relative displacement between the "free-field" soil column and the wall multiplied by a Winkler stiffness intensity, $k_y^i(z)$ [14]. The Winkler stiffness intensity term has units of force/length^3. The Winkler spring stiffness term is assumed to follow the form in Eq. 21, where k_{yH}^i is the value of the Winkler stiffness at $z = H$.

$$k_y^i(z) = k_{yH}^i \cdot f(z) \tag{21}$$

The value of k_{yH}^i is obtained by solving Eq. 22, which forces the average value of k_y^i (over the wall height) to equal the average horizontal stress divided by the average relative displacement between the "free-field" and the wall. The "free-field" displacement is defined as the soil displacement that would occur in the absence of any influence from walls (i.e., where $d\sigma_{yy}/dz = 0$ based on the equation of motion). The solution is computed for the case of a single wall retaining an infinite length soil deposit because the free-field motion is equal to that at y = ∞. The notion of a free-field displacement is more complicated for a finite-length deposit retained between two walls, because the walls influence the soil displacement everywhere in the domain. Although the antisymmetry condition imposes $\sigma_{yy} = 0$ at y = L/2, the gradient $d\sigma_{yy}/dz$ is unequal to zero along this vertical plane due to the influence of the walls. In this context, a "free-field" displacement does not exist, though it may be reasonably approximated near the center of a long soil layer (i.e., with large L/H). The resulting expression is analogous to that formulated by Kloukinas et al. [14], with the exception that in the present solution the shear modulus term in the equations is at the base of the deposit (i.e., G_H is used instead of G), the a_{oc} and a_o terms are computed using Eqs. 10a and 10b, and the b_{oc} term is introduced.

$$k_{yH}^{i} = \frac{\sigma_{yy}(0,z)}{u_y(\infty,z)\cdot f(z)} = \psi_\sigma b_{oc}\sqrt{a_{oc}^2 - a_o^2}\,\frac{G_H}{H} \tag{22}$$

Note that the "static" stiffness (i.e., $k_{yHo}^{i} = k_{yH}^{i}$ for $a_o = 0$) is linearly proportional to the product $b_{oc}a_{oc}$, and can therefore be directly scaled from Fig. 2. Equation 23 represents a regression of the resulting values of k_{yHo}^{i} for b = 0.1 to 0.9 and n = 0.05 to 0.45. In this light, b_{oc} can be viewed merely as a stiffness multiplier. Values of the normalized static stiffness are plotted as a function of Poisson's ratio for different shape functions in Fig. 8 for n = 0. 5 and b = 0.1, which are input parameters that are reasonable for cohesionless sand. Alternative shape functions have little influence on the resulting dimensionless stiffness intensity distributions.

$$k_{yHo}^{i} \approx \frac{G_H}{H}\psi_\sigma\left[1.138\cdot e^{-2.152(1-2n)-2.936b} + \frac{\pi}{2}\right] \tag{23}$$

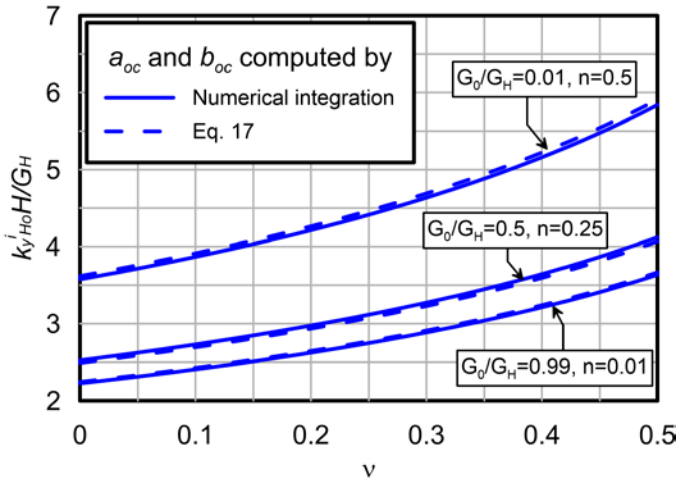

Figure 8. Profiles of normalized static Winkler stiffness intensity at the base of the wall versus Poisson ratio for various values of G_0/G_H and n.

7. Comparison of responses for inhomogeneous and homogeneous profiles

A natural question is how the Winkler stiffness intensity and seismic thrust for a specific inhomogeneous profile relates to those for an "equivalent homogeneous" profile. We define an "equivalent uniform" profile as having the same fundamental frequency as the inhomogeneous profile (both cases retain the rigid base condition). The equivalent uniform profile is obtained by solving for a_{oc}, and subsequently computing $V_{s,eq}$ using Eq. 23.

$$V_{s,eq} = \frac{V_H}{\pi} 2a_{oc} \tag{23}$$

For the equivalent homogeneous profile, $f(z) = 1$, $b_{oc} = 1$, $a_{oc,eq} = \pi/2$, and $a_{oc,eq}$ is computed using Eq. 10b with $f = 1$. The solution for $k_{y}^{i}{}_{eq}$ for an equivalent uniform profile may then be computed from Eq. 24, where $a_{o,eq} = \omega H/V_{s,eq}$. This solution is identical to that of Kloukinas et al. [17].

$$k_{y,eq}^{i} = \psi_{\sigma} \sqrt{a_{oc,eq}^2 - a_{o,eq}^2} \frac{G_{eq}}{H} \tag{24}$$

Another comparison worth making for its simplicity is to substitute G_{eq} with $G(z)$, and simply use Eq. 23 to define the profile of k_y^i. This approach neglects the difference in the physics of wave propagation for a uniform profile compared to an inhomogeneous profile due to omission of the b_{oc} term, and use of an

incorrect a_{oc} term, but is nevertheless interesting to explore to examine the nature of the resulting errors.

Example profiles are shown in Fig. 9 for b_o = 2.36, n = 0.307 and b = 0.045. The values of k_y^i are normalized by G_H/H to facilitate a fair comparison among the three approaches. The k_y^i values for the equivalent uniform profile are higher than for the inhomogeneous profile at depths shallower than about z/H = 0.45. Furthermore, the displacement is also higher in this region, thereby producing higher horizontal earth pressures. The profile using Eq. 23, but with G_{eq} set equal to $G(z)$, results in a lower value of k_y^i throughout the profile, and lower corresponding seismic earth pressures. This indicates that properly considering the physics of wave propagation is important for formulating accurate Winkler stiffness terms.

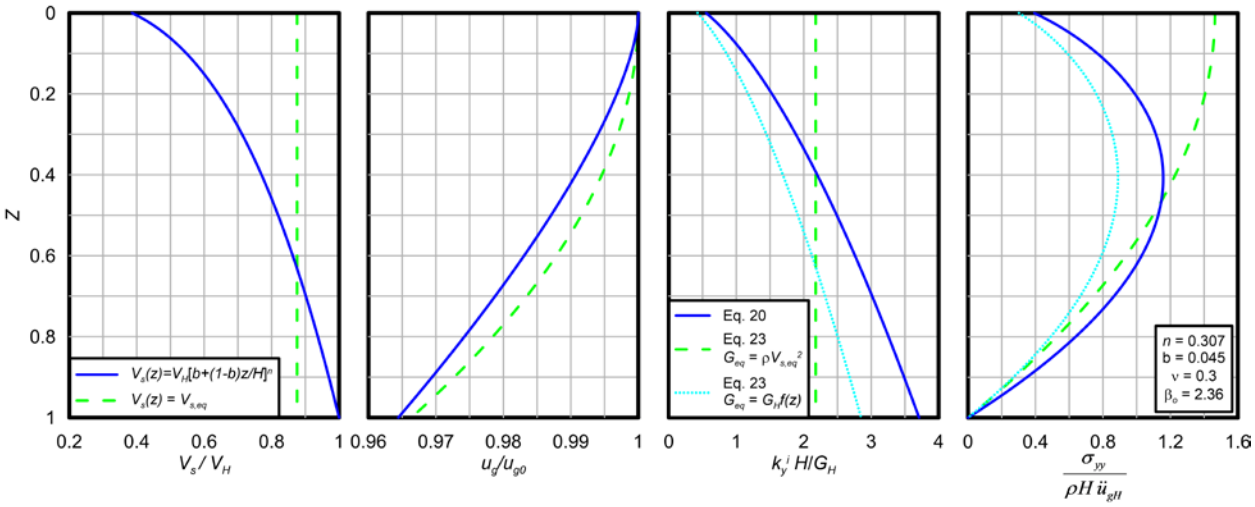

Figure 9. Comparison of response of inhomogeneous profile with "equivalent uniform" profile. Results labelled as Eq. 20 represent the proposed solution for an inhomogeneous profile with n = 0.307 and b = 0.045; halfspace results labeled as Eq. 23 match the fundamental frequency of the soil column; nonuniform results labelled as Eq. 23 substitute depth-dependent moduli into the halfspace solution of Kloukinas et al. [17].

In the special case where $a_{oc,eq} = a_{oc}$, the ratio of static stiffness intensity for the inhomogeneous case relative to the homogeneous case is given by Eq. 25. This equation elucidates that b_{oc} is a stiffness modifier accounting for inhomogeneity, and that matching the stiffness intensity for an equivalent uniform profile at all depths is not possible because the function $f(z)$ appears in the equation.

$$\frac{k_{yo}^{i}}{k_{y,eqo}^{i}} = b_{oc} \frac{G_H}{G_{eq}} f(z) \tag{25}$$

Seismic thrust values computed for a range of n and b values are presented in Fig. 10 as a ratio of the thrust for the inhomogeneous profile to that of the equivalent uniform profile. The inhomogeneous profiles produce lower seismic earth pressure resultants as compared with their "equivalent uniform" counterparts. This differential response is caused by the fact that the inhomogeneous profile is softer near the surface, where relative displacements between the soil and wall are high, and stiffer soil near the base of the wall, where relative displacements between the soil and wall are low (Brandenberg et al. [31]).

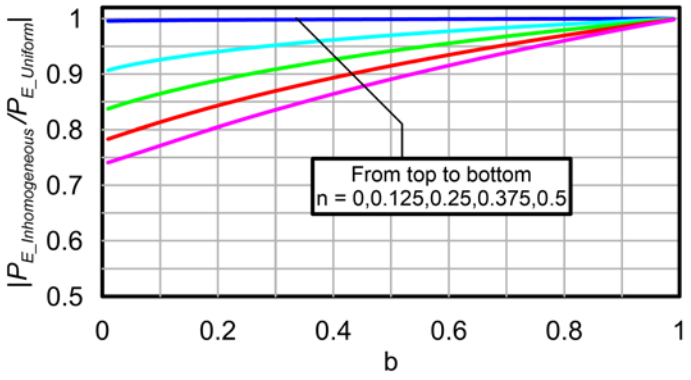

Figure 10. Influence of inhomogeneity on seismic thrust; $\nu = 0.3$, $L = \infty$.

8. Conclusions

An approximate elasto-dynamic solution was developed for seismic earth pressures acting on a single vertical rigid wall supporting a semi-infinite soil layer, and on a pair of walls spaced at a finite distance. In both cases, the soil layer is inhomogeneous and exhibits a constant Poisson's ratio and mass density. The proposed solution is simpler and easier to implement than a landmark exact analytical solution for this problem formulated by Vrettos et al. [25]. Although the proposed solution introduces errors due to the use of approximate shape functions, the assumption that vertical stresses are zero, and that the vertical displacement gradient in the horizontal direction is zero, the resulting solutions nevertheless agree quite well with exact solutions.

The solutions correspond to a rigid wall retaining an inhomogeneous soil layer resting on a rigid base. The rigid base and rigid wall assumptions do not correspond well to the boundary conditions for typical retaining walls. The infinite impedance contrast at the base of the soil layer creates significant amplification near resonance, resulting in large seismic earth pressure increments. Such amplification would not exist for the typical configuration in which the retained soil rests on a compliant base. Moreover, the rigid base assumption and the rigid wall assumption reduce the ability of the wall to conform with free-field soil displacements, thereby further increasing mobilized earth pressures. Although the present solution will overestimate seismic earth pressures for these reasons, the derivation of stiffness intensity solutions for inhomogeneous media presented herein is nonetheless a key step in the ongoing process of deriving a framework for analysis of kinematic wall response for realistic conditions, which ultimately will relax the rigid base and wall assumptions.

Acknowledgments

The authors would like to thank Professors Dimitri Beskos and Christos Vrettos for providing the raw data from their 2016 paper for the purpose of reproducing their plots for comparison with our solutions.

Appendix A

Solutions presented herein are derived using Eq. 15, which is the exact first-mode shape function for a one-dimensional continuously inhomogeneous elastic layer. In Appendix A, the solutions are derived for three other shape functions to explore the influence of shape function selection on the solutions for Winkler stiffness intensity. The first is harmonic (Eq. A1), which is an exact representation of the first-mode shape function for uniform soil; the second is parabolic (Eq. A2), which approximates the first mode shape function for uniform soil; and the third characterizes the shape of an inhomogenous soil deposit subject to a constant horizontal body force proportional to its self-weight (Eq. A3). Eq. A3 was derived by the following steps: (1) compute shear stress as a function of depth, $\tau(z) = \rho k_h z$, where $\tau(z)$ is shear stress at depth z and k_h is the horizontal body force, (2) compute shear strain as a function of depth as $\gamma(z) = \tau(z)/G_H f(z)$, (3) compute displacement at depth z by integrating shear strain from the bottom of the deposit as $u_g(z) = \int_H^z \gamma(\zeta) d\zeta$, where ζ is a dummy variable of integration, and finally (4) normalize the resulting displacement function by the surface displacement to obtain the shape function. Note that step 4 renders the shape function insensitive to selection of k_h. The detailed derivation is omitted for brevity. The shape functions are plotted in Fig. A1.

$$\Phi(Z) = \cos\left(\frac{\pi Z}{2}\right) \tag{A1}$$

$$\Phi(Z) = 1 - Z^2 \tag{A2}$$

$$\Phi(Z) = \frac{\left[b + (1-b)Z\right]^{1-2n}\left[b - (1-b)(1-2n)Z\right] - b + (1-b)(1-2n)}{b^{2\cdot(1-n)} - b + (1-b)(1-2n)} \tag{A3}$$

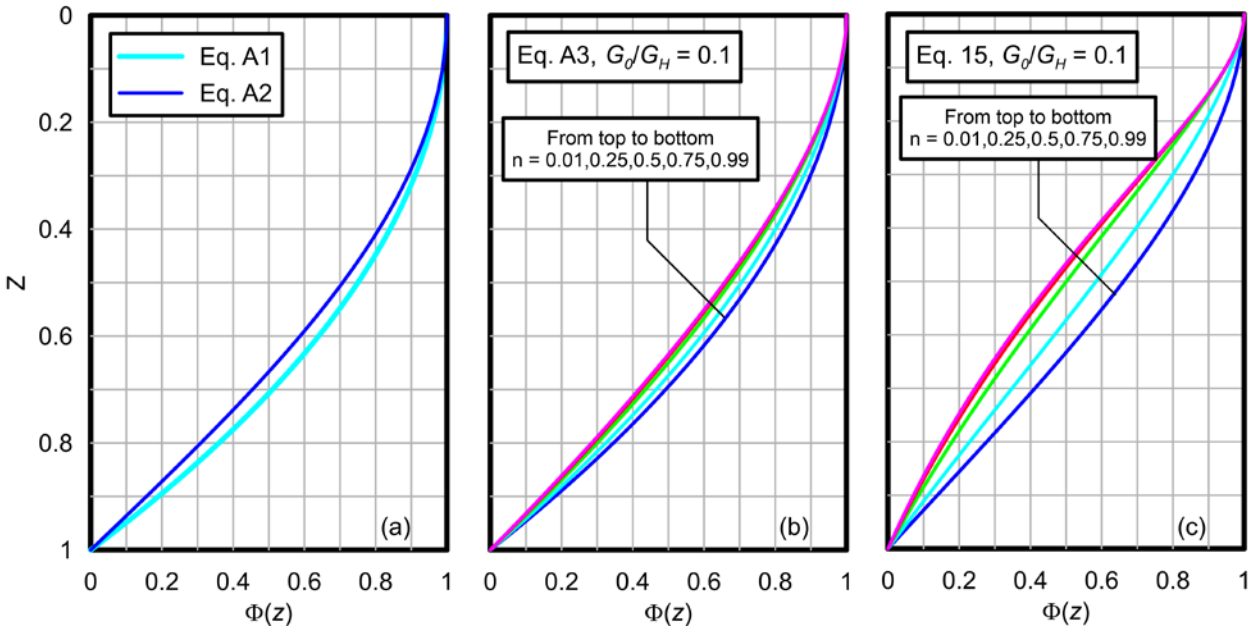

Figure A1. Shape functions corresponding to (a) harmonic (Eq. A1) and parabolic (Eq. A2) functions, (b) constant horizontal body force (Eq. A3), and (c) the exact eigenvectors for one-dimensional wave propagation.

Solutions for $\mathcal{L}$, a_{oc}, and b_{oc} computed using the shape functions in Fig. A1 are illustrated in Fig. A2. Differences among the solutions for the various shape functions increase as the degree of inhomogeneity increases (i.e., as n increases or b decreases).

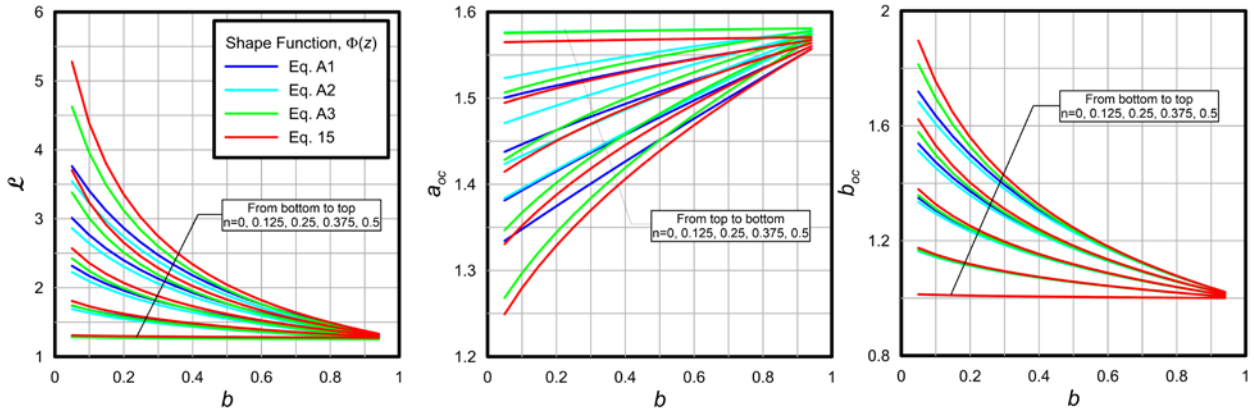

Figure A2. Solutions for $\mathcal{L}$, a_{oc}, and b_{oc} versus b for various values of n for four different shape functions.

Values of the normalized static stiffness intensity are plotted as a function of Poisson's ratio for different shape functions in Fig. A3 for n = 0.25 and b = 0.1. The shape functions defined by Eqs. A1, A2, and A3 tend to predict lower values of stiffness intensity than Eq. 15. Furthermore, Eq. 15 produces very similar results regardless of whether a_{oc} and b_{oc} are computed by numerical integration of the bounded integrals, or by the approximation provided by Eq. 17. This is further evidence that the simple closed-form expressions in Eq. 17 provide reasonably accurate values.

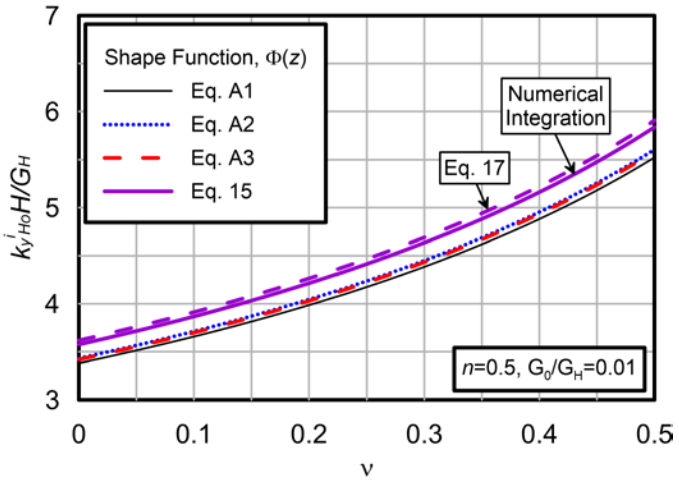

Figure A3. Normalized static Winkler stiffness intensity at the base of the wall versus Poisson ratio for four different shape functions. Furthermore, the shape function corresponding to Eq. 15 is provided based on closed-form solutions to the integrals, and according to the simplified closed-form equation given by Eq. 17.

References

[1] Okabe S. General theory of earth pressure and seismic stability of retaining wall and dam. J Jpn Soc Civ Eng 1924;12:34–41.

[2] Mononobe N, Matsuo M. On the determination of earth pressures during earthquakes. Proc. World Eng. Congr., Tokyo: Engineering Society of Japan; 1929, p. 179–87.

[3] Seed HG, Whitman RV. Design of earth retaining structures for dynamic loads. ASCE Spec. Conf.

Lateral Stress. Gr. Des. Earth Retaining Struct., Reston: American Society of Civil Engineers; 1970, p. 103–47.

[4] Chen WF, Liu XL. Limit analysis in soil mechanics. Amsterdam, Netherlands: Elsevier; 1990.

[5] Mylonakis G, Kloukinas, P. Papantonopoulos C. An alternative to the Mononobe-Okabe equation for seismic earth pressures. Soil Dyn Earthq Eng 2007;10:957–69.

[6] Xu S-Y, Shamsabadi A, Taciroglu E. Evaluation of active and passive seismic earth pressures considering internal friction and cohesion. Soil Dyn Earthq Eng 2015;70:30–47.

[7] Papagiannopoulos GA, Beskos DE, Triantafyllidis T. Seismic pressures on rigid cantilever walls retaining linear poroelastic soil : An exact solution. Soil Dyn Earthq Eng 2015;77:208–19. doi:10.1016/j.soildyn.2015.05.015.

[8] Theodorakopoulos DD, Chassiakos AP, Beskos DE. Dynamic pressures on rigid cantilever walls retaining poroelastic soil media. Part I. First method of solution. Soil Dyn Earthq Eng 2001;21:315–38. doi:10.1016/S0267-7261(01)00009-4.

[9] Theodorakopoulos DD, Chassiakos AP, Beskos DE. Dynamic pressures on rigid cantilever walls retaining poroelastic soil media. Part II. Second method of solution. Soil Dyn Earthq Eng 2001;21:339–64. doi:10.1016/S0267-7261(01)00010-0.

[10] Al Atik L, Sitar N. Seismic Earth Pressures on Cantilever Retaining Structures. J Geotech Geoenvironmental Eng 2010;136:1324–33.

[11] Mikola RG, Sitar N. Seismic earth pressures on retaining structures in cohesive soils. Berkeley, CA: 2013.

[12] Wagner N, Sitar N. On seismic response of stiff and flexible retaining structures. Soil Dyn Earthq

Eng n.d.;Published.

[13] Wood JH. Earthquake induced soil pressures on structures. Pasadena, CA: 1973.

[14] Veletsos AS, Younan AH. Dynamic soil pressures on rigid vertical walls. Earthq Engrg Struct Dyn 1994;23:275–301.

[15] Ostadan F. Seismic soil pressure for building walls - An updated approach. Soil Dyn Earthq Eng 2005;25:785–93.

[16] Brandenberg SJ, Mylonakis G, Stewart JP. Kinematic Framework for Evaluating Seismic Earth Pressures on Retaining Walls. J Geotech Geoenvironmental Eng 2015:1–10. doi:10.1061/(ASCE)GT.1943-5606.0001312.

[17] Kloukinas P, Langousis M, Mylonakis G. Simple wave solution for seismic earth pressures on nonyielding walls. J Geotech Geoenvironmental Eng 2012;128:1514–9.

[18] Hertz HR. Ueber di beruehrung elastischer koerper (on contact between elastic bodies). Gesammelte Werke (Collected Work. Vol. 1, Leipzig, Germany: 1882.

[19] Hardin BO, Richart, F.E. J. Elastic wave velocities in granular soils. J Soil Mech Found Div 1963;89:33–65.

[20] Mindlin RD, Deresiewicz H. Elastic spheres in contact under varying oblique forces. J Appl Mech 1953;20.

[21] Hardin BO, Drnevich VP. Shear modulus and damping in soils: Design equations and curves. J Soil Mech Found Div 1972;SM7:667–92.

[22] Yamada S, Hyodo M, Orense RP, Asce M, Dinesh S V. Initial Shear Modulus of Remolded Sand-Clay Mixtures 2008;134:960–71.

[23] Veletsos AS, Younan AH. Dynamic modeling and response of soil-wall systems. J Geotech Geoenvironmental Eng 1994;120:2155–79.

[24] Rovithis EN, Parashakis H, Mylonakis GE. 1D harmonic response of layered inhomogeneous soil : Analytical investigation. Soil Dyn Earthq Eng 2011;31:879–90. doi:10.1016/j.soildyn.2011.01.007.

[25] Vrettos C, Beskos DE, Triantafyllidis T. Seismic pressures on rigid cantilever walls retaining elastic continuously non-homogeneous soil : An exact solution. Soil Dyn Earthq Eng 2016;82:142–53. doi:10.1016/j.soildyn.2015.12.006.

[26] Fish J, Belytschko T. A First Course in Finite Elements. West Sussex, England: John Wiley & Sons, Ltd.; 2007.

[27] Scott RF. Foundation Analysis. Prentice Hall; 1981.

[28] Mylonakis G. Elastodynamic model for large-diameter end-bearing shafts. Soils Found 2001;41:31–44.

[29] G. A, Lemnitzer A. Dynamic impedances for laterally loaded piles using improved Takimi and Winkler formulations. Soil Dyn Earthq Eng 2017;92:279–97.

[30] Paolucci R. Shear resonance frequencies of alluvial valleys by Rayleigh's method. Earthq Spectra 1999;15:503–21.

[31] Brandenberg SJ, Agapaki E, Mylonakis G, Stewart JP. Seismic earth pressures exerted on rigid walls by vertically heterogeneous soil using Winkler method. 16th World Conf. Earthq. Eng., Santiago, Chile: 2017.